1521-0111/84/1/12–24$25.00
MOLECULAR PHARMACOLOGY

http://dx.doi.org/10.1124/mol.112.082347
Mol Pharmacol 84:12–24, July 2013

Small Molecule Inhibitors of ERCC1-XPF Protein-Protein Interaction Synergize Alkylating Agents in Cancer Cells[S]

Lars Petter Jordheim, Khaled H. Barakat, Laurence Heinrich-Balard, Eva-Laure Matera, Emeline Cros-Perrial, Karima Bouledrak, Rana El Sabeh, Rolando Perez-Pineiro, David S. Wishart, Richard Cohen, Jack Tuszynski, and Charles Dumontet

Université de Lyon (L.P.J., L.H.-B., E.-L.M., E.C.-P., K.B., R.E.S., R.C., C.D.), Université Lyon 1 (L.P.J., L.H.-B., E.-L.M., E.C.-P., K.B., R.E.S., R.C., C.D.), INSERM U1052, Centre de Recherche en Cancérologie de Lyon (L.P.J., E.-L.M., E.C.-P., K.B., R.E.S., C.D.), and CNRS UMR 5286, Centre de Recherche en Cancérologie de Lyon, Lyon, France (L.P.J., E.-L.M., E.C.-P., K.B., R.E.S., C.D.); Department of Physics, University of Alberta, Edmonton, Alberta, Canada (K.H.B., J.T.); Department of Engineering Mathematics and Physics, Fayoum University, Fayoum, Egypt (K.H.B.); MATEIS UMR-CNRS 5510, ISPB Faculté de Pharmacie, Lyon, France (L.H.-B., R.C.); Department of Biological Sciences (R.P.-P., D.S.W.) and Department of Computing Sciences, University of Alberta, Edmonton, Alberta, Canada (R.P.-P., D.S.W.); Hospices Civils de Lyon, Hôpital Edouard Herriot, Laboratoire de Biochimie et de Biologie Moléculaire, Lyon Cedex 03, France (R.C.); and Department of Oncology, University of Alberta, Edmonton, Alberta, Canada (J.T.)

Received September 11, 2012; accepted April 11, 2013

ABSTRACT

The benefit of cancer chemotherapy based on alkylating agents is limited because of the action of DNA repair enzymes, which mitigate the damage induced by these agents. The interaction between the proteins ERCC1 and XPF involves two major components of the nucleotide excision repair pathway. Here, novel inhibitors of this interaction were identified by virtual screening based on available structures with use of the National Cancer Institute diversity set and a panel of DrugBank small molecules. Subsequently, experimental validation of the in silico screening was undertaken. Top hits were evaluated on A549 and HCT116 cancer cells. In particular, the compound labeled NSC 130813 [4-[(6-chloro-2-methoxy-9-acridinyl)amino]-2-[(4-methyl-1-piperazinyl)methyl]] was shown to act synergistically with cisplatin and mitomycin C; to increase UVC-mediated cytotoxicity; to modify DNA repair as indicated by the staining of phosphorylated H2AX; and to disrupt interaction between ERCC1 and XPF in cells. In addition, using the Biacore technique, we showed that this compound interacts with the domain of XPF responsible for interaction with ERCC1. This study shows that small molecules targeting the protein-protein interaction of ERCC1 and XPF can be developed to enhance the effects of alkylating agents on cancer cells.

Introduction

Platinum derivatives are major components of the chemotherapeutic arsenal available to treat many patients with cancer. Clinical outcomes for patients treated with these drugs depend not only on the tumor type and stage but also on the biology of the targeted cancer cells. Indeed, several cellular parameters involved in pre–DNA damage mechanisms (e.g., transport deficiency and detoxification by cytoplasmic proteins), in the production and maintenance of DNA damage (e.g., DNA repair), and in the induction of cell death (e.g., DNA damage recognition and apoptotic protein expression) influence the outcome of platinum-based chemotherapy (Galluzzi et al., 2012). The clinical relevance of these modifications is not always clearly established, but a growing body of evidence indicates that proteins involved in nucleotide excision repair (NER) of DNA modulate the clinical activity of cisplatin (Hubner et al., 2011).

NER is a multistep DNA repair mechanism involving more than 30 different proteins to excise approximately 30 bases on a damaged DNA strand and to synthesize new DNA (Nouspikel, 2009). NER is activated to repair different types of DNA damage, including UV-induced bond breaks and adducts formed by platinum derivatives. By doing so, NER decreases the damage induced by platinum-based drugs, such as cisplatin, and, thus, is associated with resistance to treatment. Several NER proteins are essential for a correct DNA repair,

This work was supported by Ligue Contre le Cancer comité du Rhône; Lise og Arnfinn Hejes fond (to L.P.J.); the Allard Foundation; the Canadian Breast Cancer Foundation; and the Alberta Advanced Education and Technology (to J.A.T.).

L.P.J. and K.H.B. contributed equally to this work.

dx.doi.org/10.1124/mol.112.082347.

[S] This article has supplemental material available at molpharm.aspetjournals.org.

ABBREVIATIONS: CI_{95}, 95% combination index; DMSO, dimethylsulfoxide; ICL, interstrand crosslink; MD, molecular dynamics; MMC, mitomycin C; MTT, methylthiazoletetrazolium; NCIDS, National Cancer Institute Diversity Set; NER, nucleotide excision repair; NSC 130813, 4-[(6-chloro-2-methoxy-9-acridinyl)amino]-2-[(4-methyl-1-piperazinyl)methyl]; NSC 303812, [5,13-dihydroxy-6-(hydroxymethyl)-2,6-dimethyltetracyclo[10.3.1.01,10.02,7]hexadec-13-yl]methyl glycinate; NSC 254681, 3-acetyl-11-amino-3,6-dihydroxy-10-methoxy-5,12-dioxo-1,2,3,4,5,12-hexahydro-1-tetracenyl 3-amino-2,3,6-trideoxyhexopyranoside; PBS, phosphate-buffered saline.

and cell lines deficient in any of them are highly sensitive to UV irradiation and platinum agents. On the basis of this, it has been hypothesized that the inhibition of NER should sensitize cancer cells to these DNA-damaging agents, thus increasing their activity and eventually improving clinical outcomes.

The inhibition of NER could be achieved by several approaches, such as the development of small molecule ligands specific to the enzymes involved in the NER pathway. Another approach aims at blocking the interaction between the different elements of the NER pathway, thus preventing the repair from being completed. Indeed, the interactions among NER proteins seem to be essential for accomplishing repair, as indicated by the inhibition of NER by a peptide corresponding to the domain of XPA interacting with ERCC1 (Tsodikov et al., 2007). Such protein-protein interactions proved to be viable as druggable targets for cancer treatments, as indicated by the p53-MDM2 interaction (Shangary and Wang, 2008) and the interaction between Bcl-2 and pro-apoptotic proteins through the BH3 domain (Azmi and Mohammad, 2009). Here, we continue our in silico–based search for inhibitors targeting protein-protein interactions by focusing on those interactions that involve ERCC1 (Barakat et al., 2009, 2012). In the present study, we identified inhibitors for the ERCC1-XPF interaction. In addition to playing a key role in NER, the ERCC1-XPF complex is involved in interstrand crosslink (ICL) repair, particularly through the interaction with SLX4. Cisplatin induces mostly intrastrand adducts that are repaired by NER, but also 2–3% of ICL that are mainly responsible for the cytotoxic effect of cisplatin (Jamieson and Lippard, 1999). Other compounds inducing ICL are alkylating agents, such as mitomycin C (MMC), in which activity is also expected to be increased by the inhibition of the ERCC1-XPF interaction.

Materials and Methods

Molecular Dynamics Simulations. The model of the ERCC1-XPF C-terminal complex that we generated was based on the PDB ID 1Z00 (Tripsianes et al., 2005). The available structure represents only the interaction between the C-termini of the two proteins. Molecular dynamics (MD) simulations used the NAMD program (Phillips et al., 2005) at a mean (physiologic) temperature of 310 K, pH of 7, and the all-hydrogen AMBER99SB force-field. Protonation states of all ionizable residues were calculated using PDB ID 2PQR (Dolinsky et al., 2007). After parameterization, the XPF protein alone or in complex with ERCC1 was immersed in the center of a TIP3P water cube after adding hydrogen atoms to the initial protein structure. Only one ERCC1-XPF complex model was used for binding energy analysis. However, 20 distinct unbound XPF structures were prepared through MD simulations for statistically relevant docking analysis. The water cube's dimensions were chosen to provide at least a 20 Å buffer of water molecules around the molecular system. To neutralize and prepare the XPF-bound and XPF-free systems, respectively, under a physiologic ionic concentration, chloride and sodium ions were added by replacing water molecules with the highest electrostatic energies on their oxygen atoms. The number of counter ions for each case was calculated by first estimating the number of ions that are needed to simulate the system at pH of 7, followed by adding the number of chloride ions required to bring its charge to zero. The fully solvated proteins were then minimized and heated to the simulation temperature, with heavy restraints placed on all backbone atoms. After heating, the systems were equilibrated using periodic boundary conditions for 100 picoseconds and energy restraints reduced to zero in successive steps of the MD simulation. The simulations continued for 10 nanoseconds, during which atomic coordinates were saved to the trajectory every 2 picoseconds. The root-mean-square deviations and fluctuation coefficients (B-factors) for the protein backbone were computed over the last 5 nanoseconds of the MD simulation with use of the PTRAJ utility in AMBER10 (Case et al., 2005). A hydrogen bond was defined by a heavy donor–heavy acceptor distance $\leq$ 3.4 Å, a light donor–heavy acceptor distance $\leq$ 2.5 Å, and a deviation of less than $\pm$ 60° from linearity. For the ERCC1-XPF complex, snapshots were extracted every 2 picoseconds and used for the subsequent molecular mechanics Poisson-Boltzmann surface area binding energy analysis.

Binding Energy Analysis. Binding energy calculations used the molecular mechanics Poisson-Boltzmann surface area technique (Kollman et al., 2000; Kuhn et al., 2005). The total free energy is the sum of the mean molecular mechanical gas-phase energies (E_{MM}), solvation-free energies (G_{solv}), and entropy contributions ($-TS_{\text{solute}}$) to the binding reaction:

$$G = E_{MM} + G_{\text{solv}} - TS_{\text{solute}} \quad (1)$$

The total molecular mechanical energies can be further decomposed into contributions from electrostatic (E_{ele}), van der Waals (E_{vdw}), and internal energies (E_{int}):

$$E_{MM} = E_{\text{ele}} + E_{\text{vdw}} + E_{\text{int}} \quad (2)$$

Furthermore, the solvation-free energy can be expressed as a sum of nonelectrostatic and electrostatic contributions:

$$\Delta G_{\text{solv}} \approx \Delta G_{\text{solv}}^{\text{nonele}} + \Delta G_{\text{solv}}^{\text{ele}} \quad (3)$$

The nonelectrostatic part was approximated by a linear function of the solvent-accessible surface area:

$$\Delta G_{\text{solv}}^{\text{nonele}} = \gamma \times SASA, \quad \text{where } \gamma = 7.2 \text{ cal/mol/A}^2 \quad (4)$$

The molecular mechanical (E_{MM}) energy of each snapshot structure was calculated using the SANDER module of AMBER with all pairwise interactions included using a dielectric constant (ε) of 1. The solvation-free energy (ΔG_{solv}) is estimated as the sum of electrostatic solvation-free energy, calculated using the finite-difference solution of the Poisson-Boltzmann equation in the Adaptive Poisson-Boltzmann Solver program. The nonpolar solvation-free energy is directly proportional to the solvent-accessible surface area of the target. The solute entropy is approximated using normal mode analysis. The binding-free energy can be approximated by:

$$\Delta G^{o} = \Delta G_{\text{gas}}^{ERCC1-XPF} + \Delta G_{\text{solv}}^{ERCC1-XPF} - \left\{\Delta G_{\text{solv}}^{XPF} + \Delta G_{\text{solv}}^{ERCC1}\right\} \quad (5)$$

where ($\Delta G_{\text{gas}}^{ERCC1-XPF}$) represents the free energy per mole of the noncovalent association of the ERCC1-XPF complex in vacuum (gas phase) at 310 K, and ($-\Delta G_{\text{solv}}$) stands for the work required to transfer a molecule from its solution conformation to the same conformation in vacuum at 310 K (assuming that the binding conformation of the protein-protein complex is the same in solution and in vacuum).

Selection of a Ligand Database. The National Cancer Institute Diversity Set (NCIDS) and a panel of DrugBank small molecules (Kale et al., 1999) were used. From the approximately 2000 compounds in the NCIDS collection, a number of ligands containing rare earth elements could not be properly parameterized and were excluded, leaving a total of 1883 compounds for docking analysis. We used a version of the NCIDS formatted for use in AUTODOCK, which was prepared by the AUTODOCK Scripps team (http://autodock.scripps.edu/resources/databases). The DrugBank small molecules library is a set of 1488 Food and Drug Administration–approved drugs downloaded from the ZINC database that was expanded to 1566 by including several protonation states of some compounds.

Docking. Docking simulations on the identified site (see *Results*) of XPF were performed using the software package AUTODOCK, version 4.0 (The Scripps Research Institute, La Jolla, CA) (Morris

et al., 1998). Hydrogen atoms were added to the protein and ligands, and partial atomic charges were then assigned using the Gasteiger-Marsili method (Gasteiger and Marsili, 1980). Atomic solvation parameters were assigned to the atoms of the protein using the AUTODOCK 4.0 utility ADDSOL. Docking grid maps with $70 \times 80 \times 66$ points and grid-point spacing of 0.275 Å were centered on the binding site with use of the AUTOGRID 4.0 program (Morris et al., 1998). Rotatable bonds of each ligand were then automatically assigned using the AUTOTORS utility of AUTODOCK 4.0. Docking was performed using the Lamarckian Genetic Algorithm method with an initial population of 400 random individuals, a maximum number of 10×10^6 energy evaluations, 100 trials, 35,000 maximum generations, a mutation rate of 0.02, a crossover rate of 0.80, and the requirement that only one individual can survive into the next generation (Morris et al., 1998). A total of 20 independent virtual screening runs were performed against the full set of docked ligands with all residues of the binding site set rigid during docking experiments. This set of XPF models comprises the 20 equilibrated NMR structures (see above).

Clustering and Ranking. We used an iterative clustering technique that was developed and successfully applied in our previous studies (Barakat et al., 2009, 2010; Barakat and Tuszynski, 2011). In brief, we used an automated approach to the elbow criterion (Shao et al., 2007) with the clustering module of PTRAJ utility of AMBER10. This method exploits the fact that the percentage of variance exhibited by the data (λ) will plateau for cluster counts exceeding the optimal number.

The percentage of variance is defined by:

$$\lambda = SSR/SST \tag{6}$$

where SSR denotes the sum-of-squares regression from each cluster summed over all clusters and SST is the total sum of squares. We used the SOM algorithm as implemented in the PTRAJ utility of the AMBER10 program to cluster the docking results. This modified clustering program increases the number of clusters required until the percentage of variance exhibited by the data (λ) plateaus. This can be determined by calculating the first and second derivatives of the percentage of variance with respect to the clusters number ($d\lambda/dN$ and $d^2\lambda/dN^2$) after each attempt to increase the cluster counts. The clustering process stops at an acceptable value for these derivatives that is close to 0. Consequently, the clustering procedure depends only on the system itself and adjusts itself to arrive at the optimal clustering pattern for that specific system.

Ranking of Hits. For each virtual screening experiment, we ranked significant poses for each of the molecules contained in the database by using the results from the elbow criterion and the lowest energy that corresponds to the most populated cluster. After all poses from each ligand entry were clustered, we filtered all clusters so that only those containing at least 25% of the total population were considered as top hits. These were collected from the 20 computational experiments by first extracting the largest cluster from each individual screening, followed by ranking the clusters according to their binding energies. This produced a set of nonredundant hits ranked by their binding energies of the most populated cluster.

Cytotoxicity Assays. Human lung cancer (A549) and colon cancer (HCT116) cells were purchased from American Type Culture Collection (Manassas, VA). Cytotoxicity assays were conducted as previously described with use of the reducing activity of methylthiazoletetrazolium (MTT) to provide an estimation of cell survival (Jordheim et al., 2005). The NSC compounds (obtained from the Drug Synthesis and Chemistry Branch, Developmental Therapeutics Program, Division of Cancer Treatment and Diagnosis, National Cancer Institute, Bethesda, MD) were assessed at a final concentration of 100 μM, and the cytotoxicity was expressed as the percentage of living cells, compared with unexposed control cells. The chemical structure of F06 was confirmed by proton NMR, mass spectrometry, and high-resolution mass spectrometry (Supplemental Fig. 1). Its purity was 89.4%, as determined by high-performance liquid chromatography.

Evaluation of Synergy Effects. All compounds inducing at least an 80% decrease in cell survival at 100 μM were evaluated for synergy with cisplatin and MMC. Cells were seeded and adhered in the same manner as for cytotoxicity assays; then, different concentrations of a chemotherapeutic compound alone (0.01–4.5 μM MMC and 0.19–135 μM cisplatin for A549, 0.006–4.5 μM MMC and 0.25–180 μM cisplatin for HCT116), inhibitor alone, or a mixture with a fixed concentration ratio of the two compounds were added, and cells were incubated for another 72 hours before living cells were quantified with the MTT assay. Ratios of the two compounds used were approximately equal to $IC_{50,drug}/IC_{50,inhibitor}$. Values for IC_{50} and 95% combination index (CI_{95}) were calculated using CompuSyn software 1.0 (ComboSyn, Inc., Paramus, NJ). Synergy was defined as $CI_{95} < 0.9$, additivity for $0.9 < CI_{95} < 1.1$, and antagonism as $CI_{95} > 1.1$ (Chou and Talalay, 1984).

For human breast cancer MDA-MB-231 and MDA-MB-436 cells, similar experiments were performed with 3000 cells seeded per well, olaparib (0.25–180 μM), and F06 (0.2–810 μM) alone or in fixed concentration ratio.

UV Cell Survival Assay. Cells were seeded and adhered in 96-well plates as described above. Then, media were removed and cells were washed with phosphate-buffered saline (PBS) and exposed to UVC irradiation (40 or 80 J/m^2) in a Spectrolinker XL 1000 (Spectronics Corporation, Westbury, NY). Media without or with 0.1, 1, or 10 μM inhibitors, respectively, were added, and cells were incubated for another 72 hours before living cells were quantified using the MTT assay. Sensitization was identified as a statistically significant decrease in living cells in the presence of an inhibitor, compared with UVC-irradiated cells only. Statistical analysis was performed using Student's t test, and results are indicated with * for $P < 0.05$; ** for $P < 0.01$; and *** for $P < 0.001$.

Biacore Experiments. All experiments were performed using synthetic peptides corresponding to the interacting domains between ERCC1 and XPF (i.e., ERCC1$^{220\text{-}297}$ and XPF$^{814\text{-}905}$; Proteogenix, Oberhausbergen, France). XPF$^{814\text{-}905}$ was immobilized at flow cell 2 of a CM5 sensor chip (GE Healthcare, Little Chalfont, UK) with an amine coupling kit (GE Healthcare), as indicated by the manufacturer, using XPF$^{814\text{-}905}$ (0.05 g/l) in sodium acetate 10 mM (pH 5.5), leaving flow cell 1 as reference. ERCC1$^{220\text{-}297}$ was immobilized at flow cell 4 of the same chip and with an amine coupling using ERCC1$^{220\text{-}297}$ (0.15 g/l) in sodium acetate 10 mM (pH 4.0), leaving flow cell 3 as reference. Immobilization level was 1264 RU in flow cell 2 and 1188 RU in flow cell 4. Experiments were performed on a Biacore 2000 (GE Healthcare) with use of a PBS 5% dimethylsulfoxide (DMSO) running buffer for small molecule experiments and PBS for ERCC1-XPF interaction. Analyses were performed with a point at the end of the association phase with the maximum signal and compared with the same point in the reference channel (Fc2-Fc1 or Fc4-Fc3). A solvent correction was performed because of the presence of DMSO in the running buffer for experiments with inhibitors (Frostell-Karlsson et al., 2000).

Steady-State Fluorescence and Synchronous Fluorescence Experiments. All fluorescence spectra were collected on a PTI MODEL-MP1 spectrofluorimeter using 10-mm path length cell. For the steady-state fluorescence experiments, an excitation wavelength of 271 nm and a scan range of 282–350 nm were used. The intrinsic fluorescence of the tyrosine of XPF (2 μM; PBS buffer, pH 7.3) was monitored in the presence of increasing concentrations of F06 (10–30 μM). The data obtained from the quenching of the tyrosine intrinsic fluorescence of XPF by F06 was used to estimate the apparent binding constant for the protein-ligand complex by using the Stern-Volmer equation (van de Weert and Stell, 2011):

$$(F_o - F)/F = K_A[L]_a \tag{7}$$

where F_o and F are the fluorescence intensities in the absence and in the presence of quencher, respectively; K_A is the formation constant of

the donor-acceptor (quencher-fluorogen) complex; and $[L]_a$ is the concentration of the ligand added. Excitation and emission slits were set at 7 nm. All spectra were collected with samples having final optical densities (1 cm) less than 0.3 at maximum absorbance of added ligand and were corrected for the inner filter effect according to Eq. 8 (Lakowicz, 1999):

$$F_{corr} = F_{obs} \times 10^{\wedge}[(A_{exc} + A_{em})/2] \quad (8)$$

where F_{corr} is the corrected fluorescence, F_{obs} is the measured fluorescence, A_{exc} is the absorption value at the excitation wavelength (295 nm), and A_{em} is the absorption value at the emission wavelength (336 nm). From the slope of the linear plot of $[(F_o - F) / F]$ versus $[L]_a$, the binding constant value was estimated. The result is expressed as mean value ± S.D. ($n = 6$).

The value for the bimolecular rate quenching constant (K_q) was calculated from Eq. 9 (Lakowicz, 1999):

$$K_A = K_q \tau \quad (9)$$

where K_A is the association constant and τ is the fluorescence lifetime of the unquenched fluorophore.

Synchronous fluorescence spectra were measured at $\Delta\lambda = 20$ nm in a synchronous fluorescence wavelength range of 250–350 nm. Spectral data were collected using fluorescence software, and data analysis was performed using OriginPro 7.5 software (OriginLab, Northampton, MA).

Proximity Ligation Assay. A549 cells were incubated in the absence or presence of F06 (2 μM) and cisplatin (20 μM) for 24 hours and subsequently treated for Duolink assay (Olink Bioscience, Uppsala, Sweden), as indicated elsewhere (Coste et al., 2010), with use of ERCC1 antibody (FL-297, 1 μg; Santa Cruz Biotechnology, Santa Cruz, CA) and XPF antibody (LS-C33719, 1/1000; LifeSpan BioSciences, Seattle, WA). Dots corresponding to protein-protein interaction were counted using the Blobfinder software (The Center for Image Analysis, Uppsala University, Uppsala, Sweden) in at least 150 cells from at least five microscopic fields, and results are mean values from two independent experiments.

Immunoprecipitation. Proteins were extracted from A549 and HCT116 cells by lysis in a buffer containing 20 mM Tris-HCl (pH 6.8), 1 mM $MgCl_2$, 2 mM EGTA, 0.5% Nonidet P-40, soybean trypsin inhibitor (10 μg/ml), leupeptin (1 μg/ml), aprotinin (1 μg/ml), benzamidine (300 μg/ml), phenylmethylsulfonyl potassium (75 μg/ml), *N*-tosyl-L-pheylalanyl chloromethyl ketone (10 μg/ml), and subsequent centrifugation. Proteins (400 μg) were incubated with DMSO or F06 at 100, 200, or 500 μM at 37°C for 1 hour and then incubated with protein A/G PLUS-agarose (Santa Cruz Biotechnology) for 30 minutes at 4°C. After centrifugation and recovery of supernatant and a second incubation with A/G PLUS-Agarose, the supernatant was incubated with ERCC1 antibody (FL-297, 1 μg; Santa Cruz Biotechnology) for 2 hours at 4°C. A/G PLUS-Agarose (20 μl) was added, and the mixture was incubated overnight at 4°C on a turning wheel. After centrifugation and washing in lysis buffer, proteins were eluted twice from the beads in 15 μl of Laemmli solution at 95°C during 3 minutes. Proteins were then separated by SDS-PAGE using 10% acrylamide and transferred onto nitrocellulose membrane using iBlot system (Life Technologies, Carlsbad, CA). Membranes were incubated with XPF antibody (LS-C33719, 1/1000; LifeSpan BioSciences) and anti-murin antibody (IRdye 800CW, 1/5000; LI-COR Biosciences, Lincoln, NE), and protein expression was visualized using the Odyssey infrared system (LI-COR Biosciences).

γH2AX Immunocytochemistry. A549 cells were seeded (60,000 cells per well) in 6-well plates containing cover slips and incubated for 24 hours at 37°C; exposed to MMC (1 μM), cisplatin (50 μM), or fresh media for 1 hour; rinsed with PBS; and incubated with F06 (1 μM) or media alone for 48 hours. Cells were then washed with PBS, fixed with paraformaldehyde 4% for 15 minutes at room temperature, washed again with PBS, and blocked for 3 minutes with a buffer containing 300 mM sucrose, 3 mM $MgCl_2$, 20 mM Hepes (pH 7), 50 mM NaCl, and 0.5% Triton X-100. After washing with PBS and incubation with 1:800 dilution of anti–phospho $H2AX_{ser139}$ antibody (05636; Millipore, Billerica, MA) for 40 minutes at 37°C, cells were rinsed and incubated with a 1:100 dilution of a fluorescein isothiocyanate-conjugated secondary anti-mouse antibody (F0232; Dako Denmark, Glostrup, Denmark) for 20 minutes at 37°C. Finally, cells were rinsed with PBS and mounted with one drop of Vectashield (Vector Laboratories, Burlingame, CA). Foci were counted using a Leica DMI3000 microscope (Leica Microsystems, Wetzlar, Germany) in at least 100 cells for each condition by a person who was blinded for experimental conditions. Statistical analysis was performed using Student's *t* test, and results are indicated with * for $P <$ 0.05.

Results

MD Simulations and Binding Energy Analysis. A comparison of atomic fluctuations (as revealed by the corresponding B factor values) between the unbound-XPF and the bound-XPF structures is shown in Fig. 1. Almost all XPF residues are rigid in the bound case, compared with the

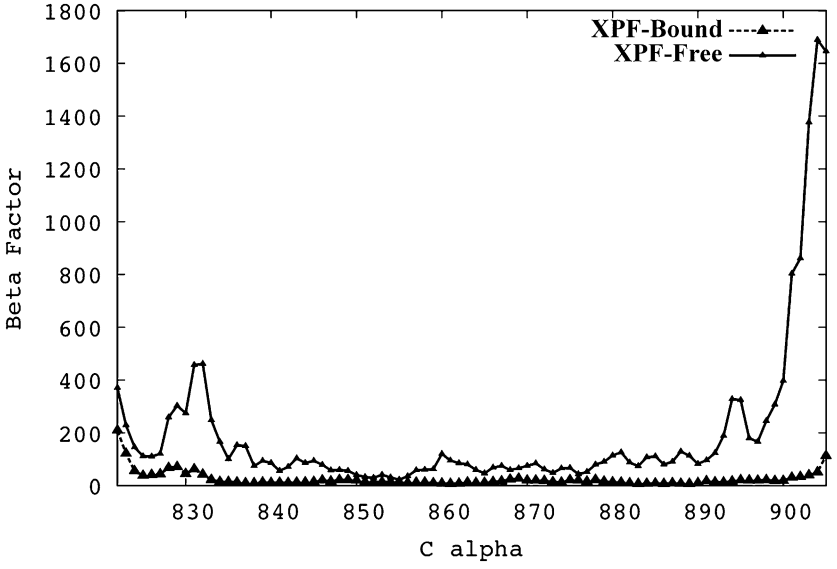

Fig. 1. Flexibility of the XPF residues. Atomic fluctuations for the free and bound XPF proteins. Binding of ERCC1 to XPF considerably stabilized the protein, indicating a wide range of protein-protein interaction.

free structure. This indicates a massive interaction between ERCC1 and XPF in which almost every residue from XPF is either interacting or being affected by an interaction with ERCC1 residues. The most flexible regions in XPF include residues 828–835, 859–862, 878–882, and 892–905. These have almost no flexibility in the bound structure, demonstrating a contribution to binding with ERCC1.

The enthalpic contribution to the binding-free energy between the two proteins was calculated and found to be exceptionally large (−123 kcal/mol). Although the solvation energy contributed passively to the interaction (298 kcal/mol), compensation from the electrostatic and van der Waals interactions dominated the overall interaction (−238 kcal/mol and −184 kcal/mol, respectively). This enthalpic term is broken down into residue-binding energy contributions, which are shown in Table 1. The ERCC1 residues shared ~50% of the total energy, with Phe293 being the residue that contributes the most to the ERCC1-XPF interaction (−11 kcal/mol). On the XPF side, Phe894 has been found to be the most strongly interacting residue by contributing −7.7 kcal/mol to the binding-free energy. With the exception of Asp839 from XPF, which disfavored the interaction by ~1 kcal/mol, the indicated residues favored the binding between ERCC1 and XPF.

By correlating the individual contributions with the positions of the different residues, one can characterize three binding interactions for XPF (Fig. 2), with only one binding pocket suitable for fitting drug candidates. When mapping these sites onto the ERCC1 side, we did not find a single pocket that would be able to fit small molecule inhibitors, even after carefully inspecting the trajectory of the XPF-ERCC1 MD simulation.

The first interaction site on the XPF protein (site I) includes residues Tyr833, Asn834, Pro837, Gln838, Met856, Lys860, Asn861, and Ile862. On the ERCC1 protein, residues 292–294 interact directly with this XPF pocket. In addition, the ERCC1 residues Val288, His290, Lys295, and Leu300 interact with residues that are close to site I. Combining the free energy contributions from the two sides shows that this portion contributes more than −50 kcal/mol. The second interaction site on XPF (site II) includes Asp839, Phe840, Lys843, Pro845, and Ala863. These residues interact with Arg234, Cys238, and Thr241 from ERCC1, and this portion contributes about −28 kcal/mol to the binding-free energy. The final XPF site (site III) comprises residues Asp888, Phe889, Thr892, Ser893, Phe894, Ala895, Val898, and Gly901, interacting with ERCC1 residues Phe231, Val232, Val235, Leu254, Gly258, Ser259, Leu260, and Glu261. These ERCC1-XPF residues contribute about −46 kcal/mol to the binding-free energy. After a careful inspection of the shapes and contributions to the binding-free energy for the three different sites, we selected site I for our virtual screening.

Relaxed Complex Scheme Virtual Screening. Here, we used a comprehensive approach that incorporates protein flexibility during the screening of ERCC1-XPF inhibitors. The

TABLE 1

Binding energy decomposition (BED) for the ERCC1-XPF interaction

Binding energy is decomposed into residue contributions. Only residues that contributed at least 1 kcal/mol are shown.

ERCC1		XPF	
Residue	BED	Residue	BED
	kcal/mol		*kcal/mol*
Met219	−1.3	Tyr833	−2.3
Phe231	−2.8	Asn834	−4.1
Val232	−2.5	Pro837	−3.9
Arg234	−2.4	Gln838	−1.2
Val235	−2.3	Asp839	−1.2
Cys238	−4.5	Phe840	−6.9
Thr241	−2.7	Lys843	−4.6
Leu254	−1.2	Pro845	−3.3
Gly258	−1.9	Met856	−1.5
Ser259	−2.9	Lys860	−2.3
Leu260	−6.3	Asn861	−3.3
Glu261	−1.0	Ile862	−3.6
Ile264	−3.0	Ala863	−2.1
Val288	−2.1	Asp888	−1.1
His290	−1.4	Phe889	−4.5
Pro292	−4.7	Thr892	−3.6
Phe293	−11.1	Ser893	−1.4
Leu294	−4.2	Phe894	−7.7
Lys295	−2.6	Ala895	−1.8
Leu300	−1.8	Val898	−1.7
		Gly901	−3.6

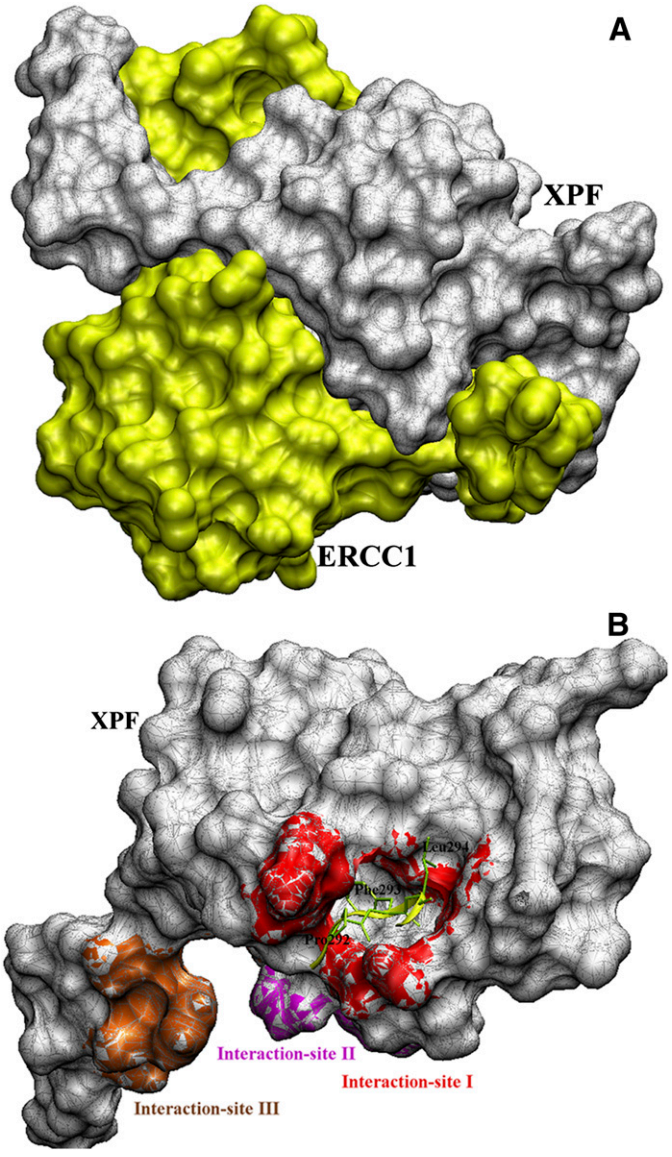

Fig. 2. The XPF-ERCC1 complex. (A) The two proteins have a massive interaction. (B) Binding energy decomposition identified three interaction sites on XPF (see text for details). The most effective site and the one that we targeted in this study is interaction-site I (red).

TABLE 2
Results from virtual screening (VS) of hit compounds

Code	Database ID	VS Score	Code	Database ID	VS Score	Code	Database ID	VS Score
		kcal/mol			*kcal/mol*			*kcal/mol*
F01	NSC 113909	−9.82	F26	NSC 37245	−9.77	F50	NSC 53396	−9.29
F02	NSC 117271	−8.31	F27	NSC 45208	−10.03	F51	NSC 74702	−10.04
F03	NSC 120672	−8.43	F28	NSC 45582	−9.78	F52	NSC 79563	−10.01
F04	NSC 120686	−8.50	F29	NSC 601364	−9.12	F53	NSC 95090	−9.68
F05	NSC 128437	−10.13	F30	NSC 633406	−9.49	F54	NSC 96021	−9.12
F06	NSC 130813	−8.23	F31	NSC 658142	−8.9	F55	NSC 108697	−10.64
F07	NSC 143099	−8.28	F32	NSC 72254	−9.46	F56	NSC 115448	−9.17
F08	NSC 143491	−9.07	F33	NSC 7524	−10.14	F57	NSC 117268	−9.09
F09	NSC 148354	−8.70	F34	NSC 82147	−8.89	F58	NSC 123994	−10.51
F10	NSC 15226	−8.38	F35	NSC 93241	−9.29	F59	NSC 127133	−9.23
F11	NSC 153625	−8.50	F36	NSC 94810	−8.72	F60	NSC 135371	−9.23
F12	NSC 16087	−9.41	F37	NSC 95278	−8.34	F61	NSC 145031	−9.43
F13	NSC 169534	−9.41	F38	NSC 97345	−9.39	F62	NSC 162404	−10.73
F14	NSC 169874	−9.01	F39	NSC 99804	−10.31	F63	NSC 168197	−9.42
F15	NSC 194598	−8.82	F40	NSC 45576	−9.07	F64	NSC 254681	−10.23
F16	NSC 211332	−8.74	F41	NSC 45583	−9.70	F65	NSC 282027	−9.41
F17	NSC 228148	−8.94	F42	ZINC03881958	−8.69	F66	NSC 303812	−9.79
F18	NSC 270156	−8.43	F43	ZINC00538312	−9.31	F67	NSC 305787	−10.09
F19	NSC 299589	−9.82	F44	NSC 3354	−9.53	F68	NSC 305821	−9.28
F20	NSC 303769	−8.78	F45	NSC 12181	−9.39	F69	NSC 307241	−9.83
F21	NSC 328087	−8.83	F46	NSC 13975	−9.24	F70	NSC 371878	−10.01
F22	NSC 339614	−8.87	F47	NSC 26645	−9.35	F71	NSC 372280	−9.34
F23	NSC 357777	−9.64	F48	NSC 35949	−10.19	F72	NSC 402959	−9.17
F24	NSC 371880	−8.8	F49	NSC 45382	−9.33	F73	NSC 407807	−9.45
F25	NSC 372294	−9.81						

method has been referred to as the relaxed complex scheme (Lin et al., 2002; Amaro et al., 2008). We performed 20 independent virtual screening runs against the 20 XPF structures present in the NMR ensemble after their free-energy equilibration using MD simulations. Top hits from each screening simulation were extracted by first clustering of their binding modes with use of the elbow criterion (see *Materials and Methods*), then ranking them through their binding energies. We defined a hit as a compound that has at least 25% of its binding modes in the same cluster and has a binding energy that is lower than −6 kcal/mol. A nonredundant list of 73 hits (Table 2) is then used for binding mode inspection and experimental validation. Because there are currently no known inhibitors of the ERCC1-XPF interaction, we were not able to use any positive controls in our relative ranking of the compounds. The binding modes of the three hits F02, F03, and F06 (Fig. 3) indicate that the

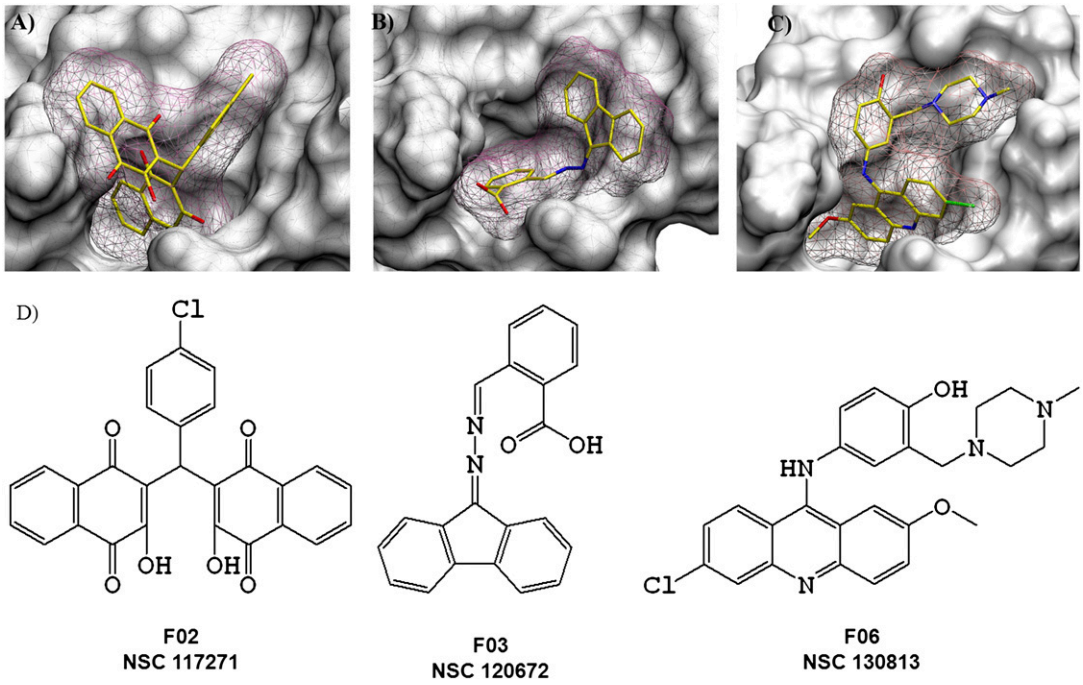

Fig. 3. Binding modes of the three hits F02 (A), F03 (B), and F06 (C) and their chemical structures (D). Atomic colors are as follows: carbon in yellow, nitrogen in blue, oxygen in red, and chlorine in green. Molecular surface grid is shown in pink around the compounds to demonstrate their fitting within the interaction site I of XPF.

compounds fit well in the XPF-binding site, suggesting a high degree of shape and feature complementarity.

Synergy between Inhibitors and Cisplatin or MMC. We chose to perform synergy studies with potential inhibitors and cisplatin on A549 and HCT116 cells in a classic MTT assay. These cell lines were chosen as models for lung and colon cancer, which represent two cancers treated with platinum derivatives. As synergy studies require compounds with intrinsic activity (here representing cytotoxicity), we only conducted these on compounds inducing at least an 80% decrease in cell survival at 100 μM. Of the 73 compounds obtained from the NCI and assessed for cell survival data, only 26 were retained for synergy analysis (unpublished data). Determination of IC_{50} indicated various activity of potential inhibitors on A549 cells (IC_{50} = 0.23–107 μM) and HCT116 cells (IC_{50} = 0.053–65.2 μM) (Supplemental Table 1). In A549 cells, we observed synergy between cisplatin and the compounds F02, F03, F06, F62, F64, F66, F67, and F68, whereas in HCT116, we observed synergy with F06, F08, F19, F48, and F64 (Fig. 4). All synergies were moderate ($0.7 < CI_{95} < 0.85$) or firm ($0.3 < CI_{95} < 0.7$). In contrast, antagonism with cisplatin was observed in A549 cells with F11, F14, F17, F19, F20, F32, F48, F53, F61, F63, F69, and F73 and in HCT116 cells with F11, F14, F17, F20, F23, F32,

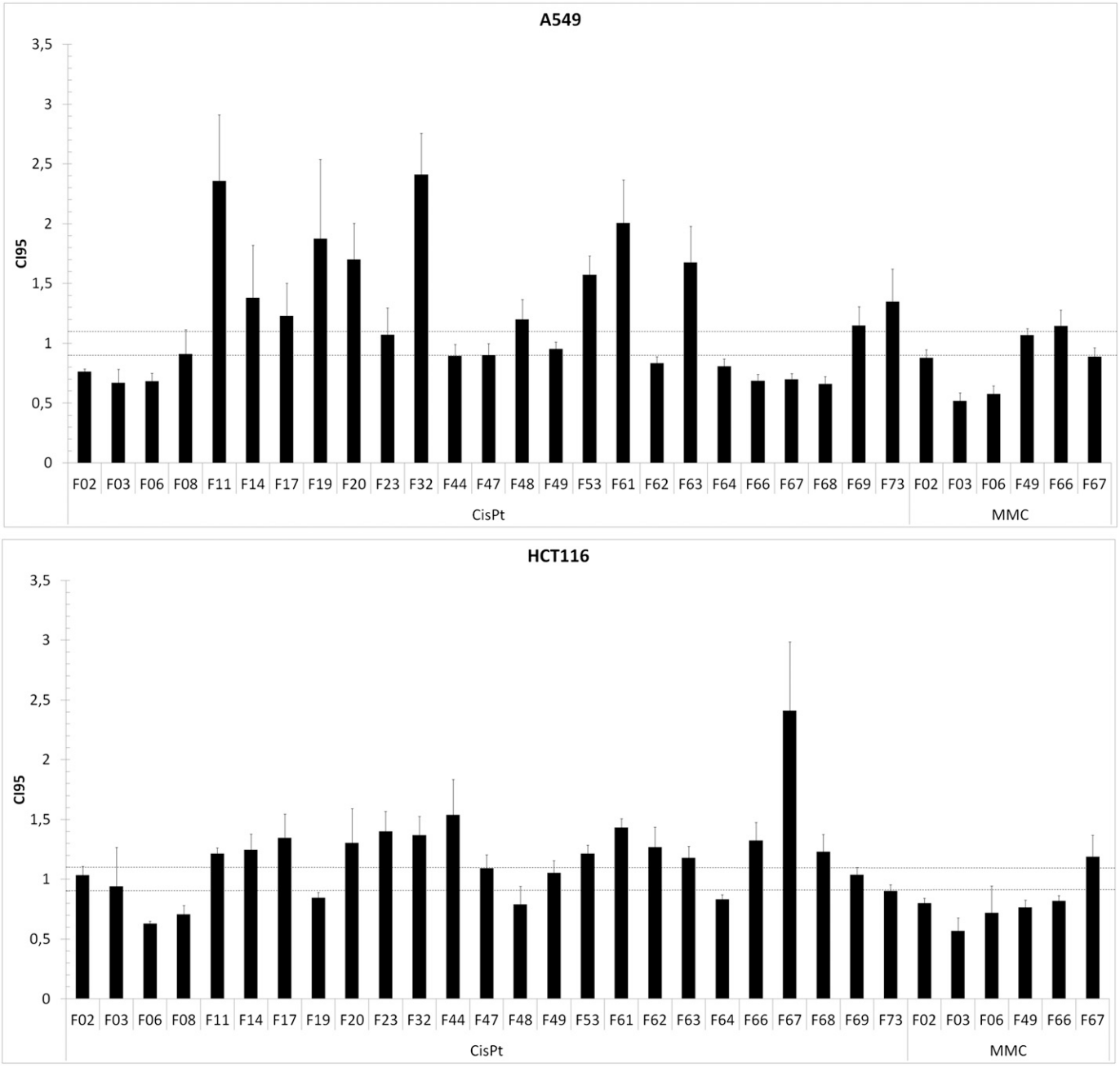

Fig. 4. CI_{95} of inhibitors and cisplatin or MMC in A549 and HCT116 cells. Results are mean values from at least seven experiments with various ratios of compounds, and error bars are S.E.M. Dotted horizontal lines indicate limits for synergy (<0.9), additivity ($0.9 < CI_{95} < 1.1$), and antagonism (>1.1).

F44, F53, F61, F62, F63, F66, F67, and F68, whereas all other combinations were additive.

Some compounds were also analyzed for synergy with MMC, another ICL-inducing agent. Here, we observed synergy with F03 and F06 and a slight synergy with F02 in A549 cells, as well as synergy with F03 and moderate synergies with F02, F06, F49, and F66 in HCT116 cells (Fig. 4).

Inhibitors Sensitize Cancer Cells to UVC Irradiation. UVC irradiation induces DNA adducts that are repaired by NER. Therefore, we used cell survival after exposure to UVC as an indirect measure of NER activity in cells incubated with or without potential inhibitors of the ERCC1-XPF interaction. Cell survival after exposure to 40 or 80 J/m^2 indicated that some compounds sensitize these cells to UVC light. In particular, for compounds showing synergy, A549 cells were sensitized by F02 (3.8-fold to 40 J/m^2; $P = 0.007$), F06 (1.8-fold to 80 J/m^2; $P = 0.02$), and F66 (1.3-fold to 40 and 80 J/m^2; $P = 0.04$; $P = 0.02$), whereas HCT116 cells only were sensitized by F02 (3.9-fold to 40 J/m^2; $P = 0.03$) (Fig. 5). Other compounds, such as F51 and F56, induced statistically significant sensitization in both cell lines at both doses of UVC (Supplemental Fig. 2).

Inhibitors Interact with Target Protein Fragments. We first confirmed the correctness of our XPF$^{814\text{-}905}$ model by showing interaction with the fragment ERCC1$^{220\text{-}297}$ (Fig. 6A). We then evaluated the interaction between selected compounds and XPF$^{814\text{-}905}$ and observed an important signature of interaction for F67 (Fig. 6B). Interaction was also observed for F06 and a weaker signal for F02 and F03. However, no interaction was observed for F15 and F16, two compounds added as negative control based on the cell survival studies, or for compounds F49 and F66. Because our SPR model did not allow us to calculate binding constants, we used fluorescence-quenching experiments. The incubation of XPF$^{814\text{-}905}$ with different concentrations of F06 decreased

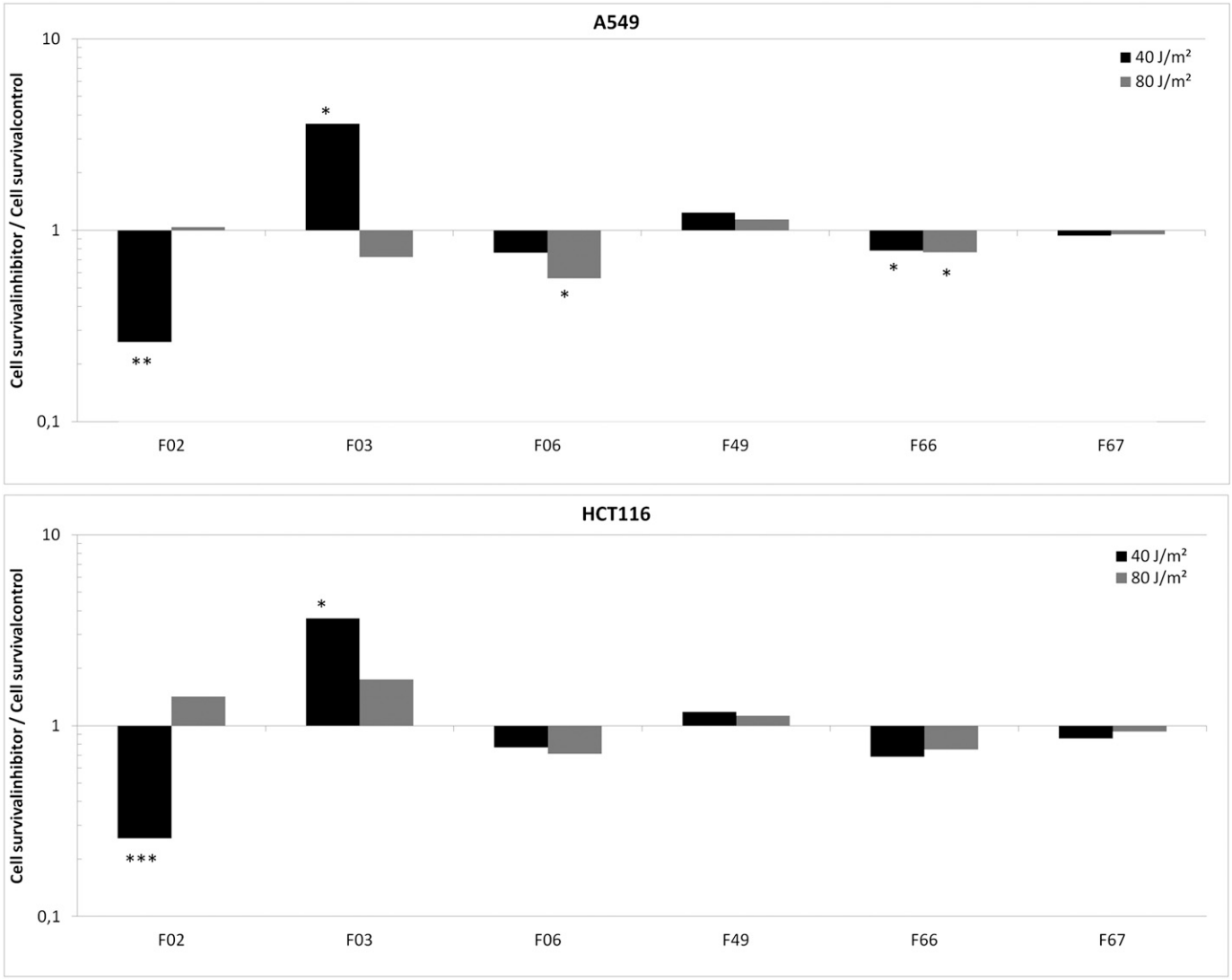

Fig. 5. Cell survival of A549 and HCT116 cells exposed to 40 and 80 J/m^2 UVC irradiation and subsequently incubated in presence or absence of potential inhibitors of ERCC1-XPF interaction. Inhibitors were used at 10 μM, except for F06 (1 μM). Results are mean values of ratios of cell survival for cells exposed and unexposed to inhibitors from four independent experiments, and error bars are S.E.M. *$P < 0.05$; **$P < 0.01$; and ***$P < 0.001$, comparing survival without and with inhibitor using Student's t test. For clarity, only molecules inducing significant difference in at least one cell model are presented. Data on all molecules are available in Supplemental Fig. 1.

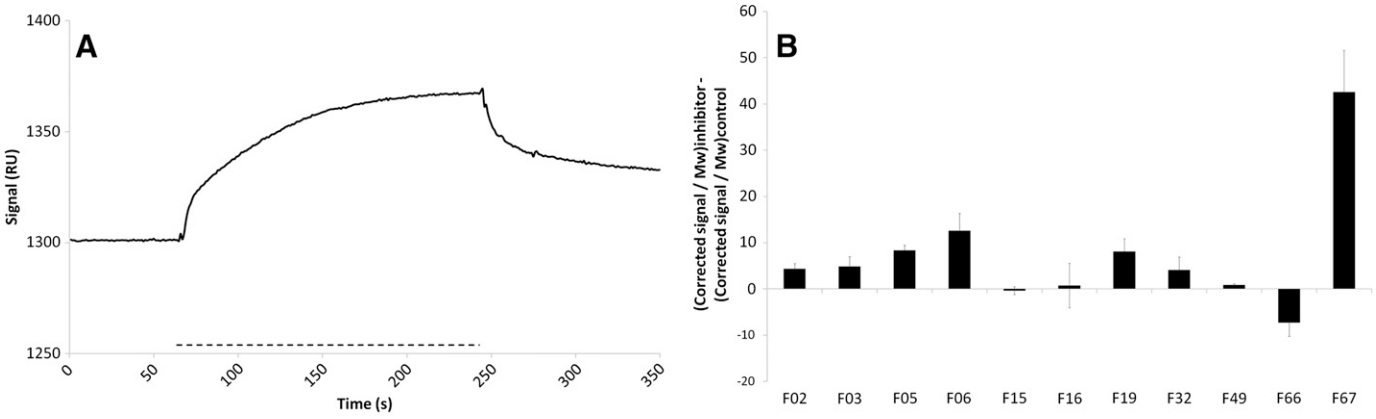

Fig. 6. (A) Sensorgram for interaction between $XPF^{814-905}$ and $ERCC1^{220-297}$. $ERCC1^{220-297}$ was injected at 10 μM in PBS containing 1 mM dithiothreitol on a chip with immobilized $XPF^{814-905}$. Dotted line indicates time of injection of $ERCC1^{220-297}$. (B) Interaction between inhibitors and $XPF^{814-905}$. Results are mean values of (corrected signal $\times$ 100/molecular weight)$_{inhibitor}$ $-$ (corrected signal $\times$ 100/molecular weight)$_{negative\ control}$ from at least three independent experiments, and error bars are S.E.M. Inhibitors were diluted at 30 μM in PBS with a final concentration of 5% DMSO. PBS 5% DMSO is considered as negative control.

the intrinsic fluorescence caused by the tyrosine residue in $XPF^{814-905}$, as shown both by steady-state fluorescence and by synchronous fluorescence spectroscopy (Fig. 7, A and B). Binding constant (K_A) and dissociation constant (K_D) between $XPF^{814-905}$ and F06 were calculated from the Stern-Volmer plot (Fig. 7C) and found to be $3.31 \times 10^4 \pm 0.0598$ l/mol and 30×10^{-6} M, respectively. The specificity of the signal was confirmed by the calculation of the bimolecular quenching rate constant (K_q), which was found to be 9.19×10^{12} Ms^{-1} and, thus, higher than K_q values obtained with nonspecific quenchers and the biopolymer (2×10^{10} Ms_{-1}).

NER Inhibitor Modifies ERCC1-XPF Interaction in Cells. To confirm modification of protein-protein interaction in a cellular context, we performed proximity ligation assay in A549 cells incubated with F06 and/or cisplatin. As expected, cisplatin increased the mean interactions per cells, as determined by the count of dots per cell (15.2 versus 35.3) (Supplemental Fig. 3; Table 3). The addition of F06 decreased the interaction between ERCC1 and XPF, both in absence (6.9 dots/cell) and in presence of cisplatin (15.2 dots/cell), showing that F06 is a potent inhibitor of the ERCC1-XPF interaction in whole cells. We confirmed this with immunoprecipitation assay in cell extracts from A549 cells incubated with different concentrations of F06 or DMSO as control. Using anti-ERCC1 as the precipitating antibody, we observed that F06 decreased the quantity of co-immunoprecipitated XPF from these cell extracts (Fig. 8), indicating that F06 is able to inhibit the interaction between XPF and ERCC1 in an environment with all cellular proteins, although at higher concentrations than expected from in vitro experiments. Similar experiments in HCT116 cells gave less concluding results (unpublished data).

NER Inhibitor Modifies Double-Stranded Break Repair. The repair of ICL involves the production of double-strand breaks that can be visualized by immunofluorescence with antibody against the phosphorylated histone H2AX. As previously shown, the inhibition of ERCC1 or XPF with siRNA modifies the kinetics of γH2AX positivity in cancer cells (Arora et al., 2010). Thus, we studied this marker in A549 cells exposed to MMC or cisplatin and incubated in the presence or absence of F06, respectively. Preliminary experiments showed that MMC and cisplatin induced positivity for γH2AX staining that was easily quantified after 48 hours (Supplemental Fig. 4). For cells exposed to MMC, the addition

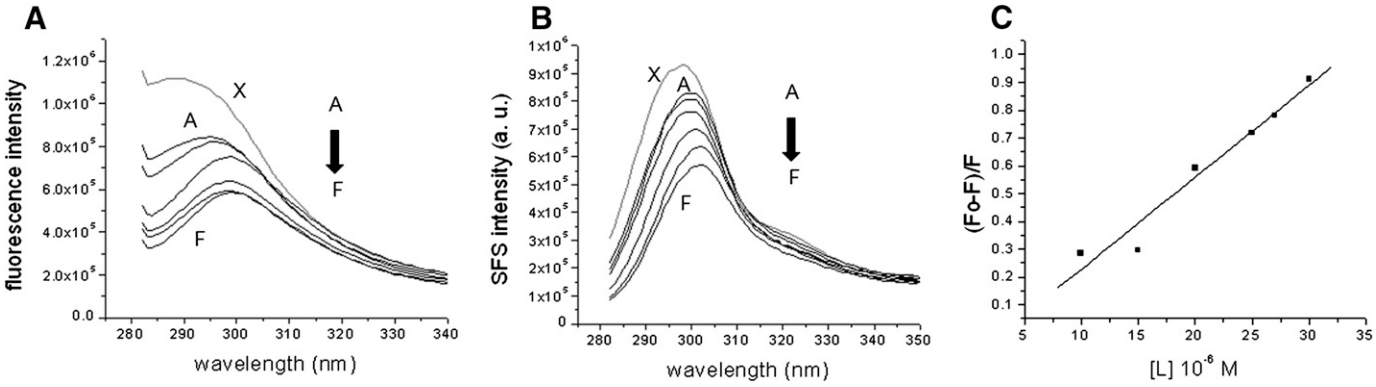

Fig. 7. Fluorescence experiments for the interaction between $XPF^{814-905}$ and F06. (A) Emission spectra of $XPF^{814-905}$ (2 μM) alone (X) and in the presence of different concentrations of F06 (A: 10, B: 15, C: 20, D: 25, E: 27, and F: 30 μM). λ_{excit} = 271 nm and excitation and emission slit width were 7 nm. (B) Synchronous fluorescence spectra of $XPF^{814-905}$ (2 μM) alone (X) and in the presence of different concentrations of F06 (A: 10, B: 15, C: 20, D: 25, E: 27, and F: 30 μM) at $\Delta\lambda$ = 20 nm. (C) The Stern-Volmer plots of fluorescence quenching of $XPF^{814-905}$ by compound F06. The value of K_A ($3.31 \times 10^4 \pm 0.0598$ l mol^{-1}) was calculated from the slope of the linear regression analysis, r = 0.9783. a.u., arbitrary unit.

TABLE 3
Results from proximity ligation assay
The numbers indicate the spots due to ERCC1-XPF interaction in A549 cells alone or incubated with 2 μM F06 and/or 20 μM cisplatin for 24 hours. Representative microscopic images are available in Supplemental Fig. 3.

Condition	NT	F06	Cisplatin	Cisplatin + F06
Spots per cell	15.2	6.9	35.3	15.2

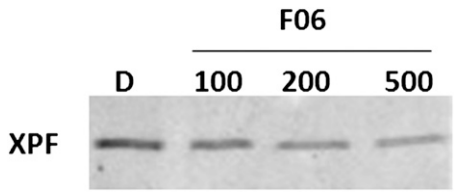

Fig. 8. Immunoprecipitation in cell extracts from A459 cells incubated with 100, 200, or 500 μM F06. The image shows a representative result of three independent experiments. D, DMSO.

of 1 μM F06 in the culture media statistically increased the percentage of cells with more than 10 foci after 48 hours, compared with cells incubated only with cell media (10% versus 4%; $P = 0.019$) (Fig. 9A). However, for cells exposed to cisplatin, no such difference was observed (Fig. 9B). The incubation with F06 alone did not induce any γH2AX staining in these conditions.

Synergy with PARP Inhibitor in BRCA1-Mutated Cells. Olaparib (AZD2281) is a PARP inhibitor that has shown interesting activity both alone and in combination with platinum derivatives in BRCA1-mutated breast cancer cells, based on the principle of synthetic lethality (Rottenberg et al., 2008). We assumed that F06 would act synergistically with olaparib in BRCA1-negative cells, because there would be an inhibition of homologous recombination, NER, ICL repair, and nonhomologous end-joining. We performed synergy analysis in both wild-type (MDA-MB-231) and BRCA1-mutated (MDA-MB-436) human breast cancer cells. As expected, sensitivity to olaparib was different in the two cell lines ($IC_{50} = 135 \pm 25$ μM versus 22 ± 6 μM in MDA-MB-231 and MDA-MB-436, respectively), whereas the sensitivity to F06 was similar in the two cell lines (2.9 ± 0.9 μM versus 3.1 ± 0.7 μM). However, we observed antagonism between olaparib and F06 in wild-type MDA-MB-231 cells ($CI_{95} = 1.7$) and synergy in BRCA1-mutated MDA-MB-436 cells ($CI_{95} = 0.7$).

Discussion

Cisplatin is a widely used cancer chemotherapy drug that is active in several tumor types, and in particular, it induces response rates above 90% in testicular cancer. However, many patients discontinue cisplatin-based treatment because of the associated toxicity or drug resistance. Therefore, the development of strategies to increase the sensitivity of resistant cancer cells to cisplatin promises to offer an enhanced clinical benefit.

The involvement of NER proteins in the clinical activity of cisplatin is now clearly established, thus constituting a target for the sensitization of cancer cells to platinum derivatives. This has been confirmed in vitro, as for example, by the induction of ERCC1 by H-Ras in human breast cancer cells (Youn et al., 2004). There, resistance to cisplatin and oxaliplatin was reversed by ERCC1-specific siRNA. Similar results were observed with the over-expression of SNAIL in human head and neck squamous cell carcinoma cell lines (FaDu, PECM-1, and CAL-27) (Hsu et al., 2010). Reduction in apoptosis in cancerous testicular germ cells (833 K) transfected with plasmid coding both ERCC1 and XPF exposed to cisplatin was also reported (Usanova et al., 2010). The same authors showed that siRNA against ERCC1 sensitized human bladder cancer cells (MGH-U1) to cisplatin with modified kinetics of γH2AX staining and increased proportion of cells in subG1. This was confirmed by individual or concomitant siRNA inhibition of ERCC1 or XPF in several human lung cancer cells (Arora et al., 2010). These studies clearly show that the modulation of ERCC1-XPF in cancer cells is associated with modified sensitivity to platinum derivatives and in γH2AX staining. Therefore, as recently suggested by others (McNeil and Melton, 2012), we used human cancer cells to evaluate the activity of potential ERCC1-XPF inhibitors and their effects on the cytotoxicity of cisplatin.

A major obstacle was encountered while identifying ERCC1-XPF inhibitors, namely an immense enthalpic contribution to the binding energy between the two proteins. Disrupting this interaction requires a quantitative understanding of its different contributions. Consequently, we first analyzed the binding mode to isolate a druggable binding site suitable for virtual screening simulations. On the basis of the energetic contributions of the different residues and their ability to form a deep pocket, we chose site I for the virtual screening. The fact that the studied inhibitors target only this site might explain why we did not observe pharmacological modifications at a level comparable to ERCC1- or XPF-deficient cells in the cells exposed to the selected inhibitors.

To identify potential inhibitors, we performed 20 virtual screening simulations with use of the 20 available NMR snapshots (Lin et al., 2002; Amaro et al., 2008). From our experience, the NCI diversity set and DrugBank provide a good starting point, especially for screening against targets with no known inhibitors. These libraries include ~3500 distinct structures that can serve as scaffolds for optimization. These structures were docked individually to the 20 XPF targets, and the top 73 hits were selected for experimental validation. An important feature present in most of our hits is the side chain that protrudes within the cavity produced by XPF-residues Tyr833, Asn834, and Pro837 that form a deep pocket, which buries the key residue Phe293. The actual interaction between compounds and these residues of XPF could be confirmed by in vitro experiments with mutant protein, and we plan to perform these experiments in the future.

For biological evaluation, we performed synergy assays to evaluate the sensitization of cisplatin by the potential inhibitors. We found several compounds that had synergistic activity with cisplatin in A549 cells and two in HCT116 cells. Two compounds are expected to be synergistic independently of ERCC1 and XPF [i.e., F66 (NSC 303812)] (Damia et al., 1992; O'Dwyer et al., 1994) and F64 (NSC 254681), a derivative of daunorubicin with IC_{50} of 0.23 and 0.05 μM on A549 and HCT116 cells, respectively. This effect is most probably not attributable to the inhibition of the ERCC1-XPF

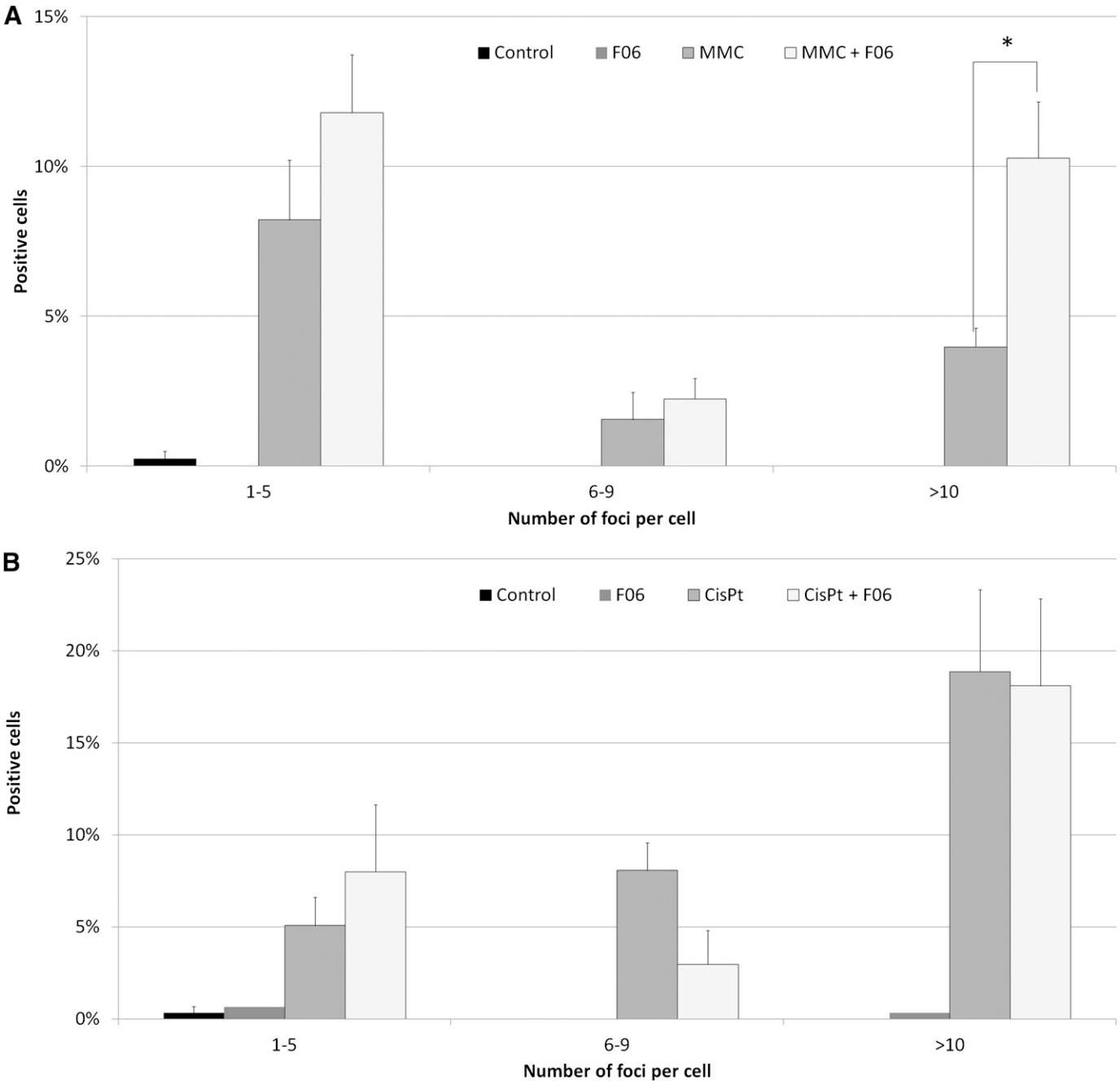

Fig. 9. Percentage of A549 cells with 1–5, 6–9, or more than 10 foci of γH2AX. Cells were exposed to 1 μM MMC (A), 50 μM cisplatin (B), or media for 1 hour and, thereafter, to 1 μM F06 or media for 48 hours. Values are mean values from four independent experiments ± S.E.M. $*P < 0.05$, with Students *t* test when comparing with cells exposed to MMC alone.

interaction. For the other compounds acting synergistically with cisplatin (F02, F03, F06, F62, F67, and F68), there was no obvious recurrent structure that could explain a common mechanism of inhibition. Because these compounds have intrinsic cytotoxicity, the synergy with cisplatin was not necessarily attributable to inhibition of the ERCC1-XPF interaction. In addition, because only compounds with intrinsic cytotoxicity can be evaluated because the effect measured was cell growth inhibition, other hits from the virtual screening might still turn out to be valid inhibitors of ERCC1 and XPF interaction.

In contrast to the other NER proteins, the ERCC1-XPF endonuclease is involved in the repair of ICL (McHugh et al., 2001; Rahn et al., 2010; Wood, 2010). This is shown by the extreme sensitivity of ERCC1- or XPF-deficient cell lines to compounds inducing ICL. The exact mechanism of this repair is not clearly understood at present, but ERCC1-XPF might be responsible for the incision of DNA at both 3′ and 5′ of the cross-link. We extended our synergy study with the ICL-inducing agent MMC. In particular, F03 and F06, which also sensitized A549 cells to cisplatin, were shown to be synergistic with MMC in these cells, thus reinforcing the hypothesis that

these molecules act by inhibition of the interaction between ERCC1 and XPF.

To reveal the mechanism of action of the potential inhibitors of the ERCC1-XPF interaction, we evaluated the interaction between these compounds and XPF with use of a fragment of XPF corresponding to the targeted domain of the interaction with ERCC1. Biacore experiments are based on the detection and the quantification of the interaction between one compound immobilized on a sensor chip (here, the XPF fragment) and another compound solubilized in a running buffer (here, the inhibitors). Our results show that, in particular, F67 and F06 interact with $XPF^{814-905}$, suggesting that the effect observed on the cell models with F06 is attributable to an interaction with NER proteins. F06 was also shown to interact with ERCC1, although at higher concentrations than for XPF. F67 induced a strong signal of interaction with $XPF^{814-905}$, even though it showed only synergy with cisplatin in A549 cells and not with other compounds or in HCT116 cells. This indicates that its interaction with the XPF fragment is not necessarily inhibiting the protein-protein interaction. Concerning F06, we were able to show a specific and saturable interaction with XPF and to determine the binding parameters of the interaction by fluorescence quenching experiments. The fact that we were not able to quantify this interaction by SPR might be attributable to the differences in structural conformation of the XPF fragment immobilized on the sensor chip, compared with the soluble XPF fragment used in fluorescence quenching experiments. The role of F06 on the inhibition of the interaction between ERCC1 and XPF was finally confirmed both by proximity ligation assays and by immunoprecipitation. The proximity ligation assay clearly confirmed the ability of this compound to act on ERCC1 and XPF in cells.

There is a negative correlation between cell survival after cisplatin exposure and the γH2AX expression in cancer cells (Olive and Banath, 2009). Niedernhofer et al. (2004) showed in ERCC1-deficient mouse embryonic stem cells that ERCC1-XPF is not required for the formation of double-strand breaks after exposure to ICL-inducing agents. However, ICL repair is largely slowed down in ERCC1-deficient cells, and the kinetics of the γH2AX signal was largely modified, lasting for more than 72 hours in ERCC1-deficient cells, compared with 12–24 hours in wild-type cells. Such variations were also observed in cancer cells transfected with siRNA against ERCC1 or XPF and exposed to cisplatin (Arora et al., 2010; Usanova et al., 2010). Our results on γH2AX staining are consistent with previous observations concerning the down-regulation of ERCC1 and XPF, even though the effect is somehow weaker. This can be attributable to the weaker inhibition caused by F06, compared with siRNA against ERCC1 or XPF, which further motivates us to search for more active analogs of F06.

Synthetic lethality is a concept based on targeting a pathway that has become crucial in a cell line because of the inactivation of another pathway. A well-described example involves PARP in BRCA1- or BRCA2-deficient cells. Because ERCC1-XPF is involved in DNA repair other than PARP and BRCA, NER inhibition should additionally increase the activity of PARP inhibitors in BRCA-mutated cells. As shown, the association of olaparib and F06 is only synergistic in BRCA1-deficient breast cancer cells. This is the first observation of such an additional effect by targeting NER. Confirmation of the role of ERCC1-XPF in this synergy is still needed.

We did not observe a clear correlation between the results obtained with different techniques. This discrepancy among intrinsic cytotoxicity, synergistic potential, UVC sensitization, and interaction with the XPF fragment can be explained by the nonspecificity of the compounds. Indeed, some compounds might have several distinct molecular effects on cancer cells and elicit various responses. Hypothetically, the interaction between some compounds and XPF could increase the affinity for ERCC1, thus inducing antagonsim with cisplatin or MMC. Although specific molecules are most often preferred in studies of this type, the most important finding reported here is that our hit compound is able to increase the cytotoxicity of cisplatin in cancer cells.

We have focused on inhibitors of NER acting through the inhibition of a protein-protein interaction and demonstrated that F06 (NSC 130813, NERI02) interacts with XPF, synergizes cancer cells to cisplatin and MMC, modifies DNA repair, interacts with ERCC1 and XPF in vitro, and decreases the interaction between ERCC1 and XPF in cells and cell extracts. This confirms the hypothesis that the inhibition of NER by targeting protein-protein interactions sensitizes the cytotoxic activity of alkylating agents. NERI02 should be subjected to derivatization to optimize its action.

Acknowledgments

The authors thank Nicolas Foray for assistance on γH2AX assessment, Amandine Roux for Biacore experiments, and Suzanne Peyrottes for structure and purity determinations. NAMD was developed by the Theoretical and Computational Biophysics Group in the Beckman Institute for Advanced Science and Technology at the University of Illinois at Urbana-Champaign.

Authorship Contributions

Participated in the research design: Jordheim, Barakat, Heinrich-Balard, Matera, Cros-Perrial, Bouledrak, El Sabeh, Perez-Pineiro, Wishart, Cohen, Tuszynski, Dumontet.

Conducted experiments: Jordheim, Barakat, Heinrich-Balard, Matera, Cros-Perrial, Bouledrak, El Sabeh, Perez-Pineiro.

Performed data analysis: Jordheim, Barakat, Heinrich-Balard, Matera, Cros-Perrial, Bouledrak, El Sabeh, Perez-Pineiro, Tuszynski, Dumontet.

Wrote or contributed to the writing of the manuscript: Jordheim, Barakat, Heinrich-Balard, Wishart, Cohen, Tuszynski, Dumontet.

References

Amaro RE, Baron R, and McCammon JA (2008) An improved relaxed complex scheme for receptor flexibility in computer-aided drug design. *J Comput Aided Mol Des* **22**:693–705.

Arora S, Kothandapani A, Tillison K, Kalman-Maltese V, and Patrick SM (2010) Downregulation of XPF-ERCC1 enhances cisplatin efficacy in cancer cells. *DNA Repair (Amst)* **9**:745–753.

Azmi AS and Mohammad RM (2009) Non-peptidic small molecule inhibitors against Bcl-2 for cancer therapy. *J Cell Physiol* **218**:13–21.

Barakat K, Mane J, Friesen D, and Tuszynski J (2010) Ensemble-based virtual screening reveals dual-inhibitors for the p53-MDM2/MDMX interactions. *J Mol Graph Model* **28**:555–568.

Barakat K and Tuszynski J (2011) Relaxed complex scheme suggests novel inhibitors for the lyase activity of DNA polymerase beta. *J Mol Graph Model* **29**:702–716.

Barakat KH, Jordheim LP, Perez-Pineiro R, Wishart D, Dumontet C, and Tuszynski JA (2012) Virtual screening and biological evaluation of inhibitors targeting the XPA-ERCC1 interaction. *PLoS ONE* **7**:e51329.

Barakat KH, Torin Huzil J, Luchko T, Jordheim L, Dumontet C, and Tuszynski J (2009) Characterization of an inhibitory dynamic pharmacophore for the ERCC1-XPA interaction using a combined molecular dynamics and virtual screening approach. *J Mol Graph Model* **28**:113–130.

Case DA, Cheatham T, Darden T, Gohlke H, Luo R, Merz KM Jr, Onufriev A, Simmerling C, Wang B, and Woods R (2005) The Amber biomolecular simulation programs. *J Comput Chem* **26**:1668–1688.

Chou TC and Talalay P (1984) Quantitative analysis of dose-effect relationships: the combined effects of multiple drugs or enzyme inhibitors. *Adv Enzyme Regul* **22**: 27–55.

Coste I, Le Corf K, Kfoury A, Hmitou I, Druillennec S, Hainaut P, Eychene A, Lebecque S, and Renno T (2010) Dual function of MyD88 in RAS signaling and inflammation, leading to mouse and human cell transformation. *J Clin Invest* **120**:3663–3667.

Damia G, Tagliabue G, Zucchetti M, Davoli E, Sessa C, Cavalli F, and D'Incalci M (1992) Activity of aphidicolin glycinate alone or in combination with cisplatin in a murine ovarian tumor resistant to cisplatin. *Cancer Chemother Pharmacol* **30**: 459–464.

Dolinsky TJ, Czodrowski P, Li H, Nielsen JE, Jensen JH, Klebe G, and Baker NA (2007) PDB2PQR: expanding and upgrading automated preparation of biomolecular structures for molecular simulations. *Nucleic Acids Res* **35** (Web Server issue):W522-5.

Frostell-Karlsson A, Remaeus A, Roos H, Andersson K, Borg P, Hämäläinen M, and Karlsson R (2000) Biosensor analysis of the interaction between immobilized human serum albumin and drug compounds for prediction of human serum albumin binding levels. *J Med Chem* **43**:1986–1992.

Galluzzi L, Senovilla L, Vitale I, Michels J, Martins I, Kepp O, Castedo M, and Kroemer G (2012) Molecular mechanisms of cisplatin resistance. *Oncogene* **31**: 1869–1883.

Gasteiger J and Marsili M (1980) Iterative partial equalization of orbital electronegativity: a rapid access to atomic charges. *Tetrahedron* **36**:3219–3228.

Hsu DS, Lan HY, Huang CH, Tai SK, Chang SY, Tsai TL, Chang CC, Tzeng CH, Wu KJ, and Kao JY et al. (2010) Regulation of excision repair cross-complementation group 1 by Snail contributes to cisplatin resistance in head and neck cancer. *Clin Cancer Res* **16**:4561–4571.

Hubner RA, Riley RD, Billingham LJ, and Popat S (2011) Excision repair cross-complementation group 1 (ERCC1) status and lung cancer outcomes: a meta-analysis of published studies and recommendations. *PLoS ONE* **6**:e25164.

Jamieson ER and Lippard SJ (1999) Structure, Recognition, and Processing of Cisplatin-DNA Adducts. *Chem Rev* **99**:2467–2498.

Jordheim LP, Guittet O, Lepoivre M, Galmarini CM, and Dumontet C (2005) Increased expression of the large subunit of ribonucleotide reductase is involved in resistance to gemcitabine in human mammary adenocarcinoma cells. *Mol Cancer Ther* **4**:1268–1276.

Kale L, Skeel R, Bhandarkar M, Brunner R, Gursoy A, Krawetz N, Phillips J, Shinozaki A, Varadarajan K, and Schulten K (1999) NAMD2: Greater Scalability for Parallel Molecular Dynamics. *J Comput Phys* **151**:283–312.

Kollman PA, Massova I, Reyes C, Kuhn B, Huo S, Chong L, Lee M, Lee T, Duan Y, and Wang W et al. (2000) Calculating structures and free energies of complex molecules: combining molecular mechanics and continuum models. *Acc Chem Res* **33**:889–897.

Kuhn B, Gerber P, Schulz-Gasch T, and Stahl M (2005) Validation and use of the MM-PBSA approach for drug discovery. *J Med Chem* **48**:4040–4048.

Lakowicz JR(1999) *Principles of fluorescence spectroscopy*, Second ed. Kluwer Academic/Plenum, New York.

Lin JH, Perryman AL, Schames JR, and McCammon JA (2002) Computational drug design accommodating receptor flexibility: the relaxed complex scheme. *J Am Chem Soc* **124**:5632–5633.

McHugh PJ, Spanswick VJ, and Hartley JA (2001) Repair of DNA interstrand crosslinks: molecular mechanisms and clinical relevance. *Lancet Oncol* **2**:483–490.

McNeil EM and Melton DW (2012) DNA repair endonuclease ERCC1-XPF as a novel therapeutic target to overcome chemoresistance in cancer therapy. *Nucleic Acids Res* **40**:9990–10004.

Morris GM, Goodsell DS, Halliday RS, Huey R, Hart WE, Belew RK, and Olson AJ (1998) Automated docking using a Lamarckian genetic algorithm and an empirical binding free energy function. *J Comput Chem* **19**:1639–1662.

Niedernhofer LJ, Odijk H, Budzowska M, van Drunen E, Maas A, Theil AF, de Wit J, Jaspers NG, Beverloo HB, and Hoeijmakers JH et al. (2004) The structure-specific endonuclease Ercc1-Xpf is required to resolve DNA interstrand cross-link-induced double-strand breaks. *Mol Cell Biol* **24**:5776–5787.

Nouspikel T (2009) DNA repair in mammalian cells : Nucleotide excision repair: variations on versatility. *Cell Mol Life Sci* **66**:994–1009.

O'Dwyer PJ, Moyer JD, Suffness M, Harrison SD, Jr, Cysyk R, Hamilton TC, and Plowman J (1994) Antitumor activity and biochemical effects of aphidicolin glycinate (NSC 303812) alone and in combination with cisplatin in vivo. *Cancer Res* **54**:724–729.

Olive PL and Banáth JP (2009) Kinetics of H2AX phosphorylation after exposure to cisplatin. *Cytometry B Clin Cytom* **76**:79–90.

Phillips JC, Braun R, Wang W, Gumbart J, Tajkhorshid E, Villa E, Chipot C, Skeel RD, Kale L, and Schulten K (2005) Scalable molecular dynamics with NAMD. *J Comput Chem* **26**:1781–1802.

Rahn JJ, Adair GM, and Nairn RS (2010) Multiple roles of ERCC1-XPF in mammalian interstrand crosslink repair. *Environ Mol Mutagen* **51**:567–581.

Rottenberg S, Jaspers JE, Kersbergen A, van der Burg E, Nygren AO, Zander SA, Derksen PW, de Bruin M, Zevenhoven J, and Lau A et al. (2008) High sensitivity of BRCA1-deficient mammary tumors to the PARP inhibitor AZD2281 alone and in combination with platinum drugs. *Proc Natl Acad Sci USA* **105**: 17079–17084.

Shangary S and Wang S (2008) Targeting the MDM2-p53 interaction for cancer therapy. *Clin Cancer Res* **14**:5318–5324.

Shao J, Tanner SW, Thompson N, and Cheatham TE, 3rd (2007) Clustering Molecular Dynamics Trajectories: 1. Characterizing the Performance of Different Clustering Algorithms. *J Chem Theory Comput* **3**:2312–2334.

Tripsianes K, Folkers G, Ab E, Das D, Odijk H, Jaspers NG, Hoeijmakers JH, Kaptein R, and Boelens R (2005) The structure of the human ERCC1/XPF interaction domains reveals a complementary role for the two proteins in nucleotide excision repair. *Structure* **13**:1849–1858.

Tsodikov OV, Ivanov D, Orelli B, Staresincic L, Shoshani I, Oberman R, Schärer OD, Wagner G, and Ellenberger T (2007) Structural basis for the recruitment of ERCC1-XPF to nucleotide excision repair complexes by XPA. *EMBO J* **26**: 4768–4776.

Usanova S, Piée-Staffa A, Sied U, Thomale J, Schneider A, Kaina B, and Köberle B (2010) Cisplatin sensitivity of testis tumour cells is due to deficiency in interstrand-crosslink repair and low ERCC1-XPF expression. *Mol Cancer* **9**: 248.

van de Weert M and Stell L (2011) Fluorescence quenching and ligand binding: A critical discussion of a popular methodology. *J Mol Struct* **998**:144–150.

Wood RD (2010) Mammalian nucleotide excision repair proteins and interstrand crosslink repair. *Environ Mol Mutagen* **51**:520–526.

Youn CK, Kim MH, Cho HJ, Kim HB, Chang IY, Chung MH, and You HJ (2004) Oncogenic H-Ras up-regulates expression of ERCC1 to protect cells from platinum-based anticancer agents. *Cancer Res* **64**:4849–4857.

Address correspondence to: Lars Petter Jordheim, Equipe Anticorps-Anticancer, Centre de Recherche en Cancérologie de Lyon, INSERM U1052–CNRS UMR 5286, Faculté Rockefeller, 8 Avenue Rockefeller, 69008 Lyon, France. E-mail: lars-petter.jordheim@univ-lyon1.fr